analytical chemistry

Article

Cite This: Anal. Chem. 2018, 90, 5930−5937

pubs.acs.org/ac

Exploration of Nanoparticle-Mediated Photothermal Effect of TMB-H_2O_2 Colorimetric System and Its Application in a Visual Quantitative Photothermal Immunoassay

Guanglei Fu,[†] Sharma T. Sanjay,[†] Wan Zhou,[†] Rolf A. Brekken,[‡] Robert A. Kirken,[§] and XiuJun Li*[,†,∥,⊥]

[†]Department of Chemistry and Biochemistry, University of Texas at El Paso, 500 West University Avenue, El Paso, Texas 79968, United States

[‡]Hamon Center for Therapeutic Oncology Research, Departments of Surgery and Pharmacology, University of Texas Southwestern Medical Center, 6000 Harry Hines Blvd, Dallas, Texas 75390, United States

[§]Department of Biological Sciences, University of Texas at El Paso, 500 West University Avenue, El Paso, Texas 79968, United States

[∥]Biomedical Engineering, Border Biomedical Research Center, University of Texas at El Paso, 500 West University Avenue, El Paso, Texas 79968, United States

[⊥]Environmental Science and Engineering, University of Texas at El Paso, 500 West University Avenue, El Paso, Texas 79968, United States

Supporting Information

ABSTRACT: The exploration of new physical and chemical properties of materials and their innovative application in different fields are of great importance to advance analytical chemistry, material science, and other important fields. Herein, we, for the first time, discovered the photothermal effect of an iron oxide nanoparticles (NPs)-mediated TMB (3,3′,5,5′-tetramethylbenzidine)-H_2O_2 colorimetric system, and applied it toward the development of a new NP-mediated photothermal immunoassay platform for visual quantitative biomolecule detection using a thermometer as the signal reader. Using a sandwich-type proof-of-concept immunoassay, we found that the charge transfer complex of the iron oxide NPs-mediated one-electron oxidation product of TMB (oxidized TMB) exhibited not only color changes, but also a strong near-infrared (NIR) laser-driven photothermal effect. Hence, oxidized TMB was explored as a new sensitive photothermal probe to convert the immunoassay signal into heat through the near-infrared laser-driven photothermal effect, enabling simple photothermal immunoassay using a thermometer. Based on the new iron oxide NPs-mediated TMB-H_2O_2 photothermal immunoassay platform, prostate-specific antigen (PSA) as a model biomarker can be detected at a concentration as low as 1.0 ng·mL^{-1} in normal human serum. The discovered photothermal effect of the colorimetric system and the developed new photothermal immunoassay platform open up a new horizon for affordable detection of disease biomarkers and have great potential for other important material and biomedical applications of interest.

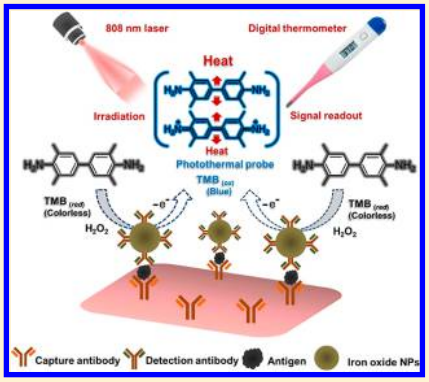

The photothermal effect has attracted intensive research interest in a number of fields due to the unique photothermal conversion property.[1,2] Significantly, the nanomaterial-mediated photothermal effect has been extensively applied for photothermal therapy of cancers using the hyperthermia effect generated by photothermal agents.[3−9] Various materials such as nanomaterials and small organic molecules, which can absorb and convert certain wavelengths of light into heat, have been explored as photothermal agents.[10−15] During the photothermal conversion process of these photothermal agents, a common thermometer, one of the simplest and the most widely used household tools, can be used to measure the photothermal effect-induced heat in a quantitative manner. Guided by this hypothesis, due to the ease of a thermometer for the signal readout, development of a simple photothermal effect-based quantitative readout method using a thermometer is particularly promising in various applications, especially in point-of-care (POC) detection of biomolecules. This will not only expand the applications of photothermal effects, but also address a bottleneck problem of conventional methods for biomolecular detection in resource-limited settings.

Biomolecular detection plays a vital role in disease diagnosis.[16,17] Different biomolecular immunoassay methods involving fluorescence,[18] surface plasmon resonance,[19,20] electrochemistry,[21] and chemiluminescence[22] have been widely used for disease diagnosis and bioanalysis. Unfortunately, most traditional biomolecule detection methods are frequently confronted with limitations to their wide application in

Received: February 21, 2018
Accepted: April 11, 2018
Published: April 11, 2018

DOI: 10.1021/acs.analchem.8b00842
Anal. Chem. 2018, 90, 5930−5937

resource-poor settings, such as small clinics in developing nations, POC detection, and field detection. In particular, the dependence of the assay readout method on complex, expensive, and bulky analytical instruments,[23,24] such as microplate readers, becomes one of the most challengeable limitations of these methods for simple, low-cost, and portable POC detection.[25] Hence, there is a critical need for the development of new immunoassay strategies with simple low-cost readout methods and high portability in order to meet the requirement of modern clinical diagnostics in resource-limited settings.[26−28] By innovatively introducing the nanoparticle (NP)-mediated photothermal effect into bioassays, our research group previously developed a new photothermal bioanalysis concept using a thermometer as the quantitative signal reader.[29] The thermometer-based photothermal bioanalysis concept provides new possibilities to address those problems of traditional immunoassay methods. However, the required material conversion procedure from the weak photothermal agent (i.e., iron oxide NPs) to the strong photothermal probe (i.e., Prussian blue NPs) makes the assay fairly complicated. Thus, the exploration of new photothermal probes with simpler derivation but broader biochemical applications is crucial to advance instrument-free bioanalysis and POC detection.

The nanomaterial-mediated colorimetric assay is an attractive method for POC detection due to its unmatched advantages of simplicity.[30−33] A variety of colorimetric assays based on different nanomaterial platforms[34,35] have been extensively developed for immunoassay. Among various colorimetric assay systems, the 3,3′,5,5′-tetramethylbenzidine (TMB)-H_2O_2 colorimetric system catalyzed by horseradish peroxidase (HRP) or other nanomaterials, such as iron oxide NPs, has been one of the widely used ELISA systems.[36] Although these colorimetric assays have shown considerable promise for naked eye-based qualitative detection (yes or no answers), the further requirement of advanced analytical instruments, such as a UV−vis absorption spectrometer,[23] is generally indispensable to achieve accurate quantitative readouts, limiting the assay's potential for low-cost disease diagnosis. Therefore, substantial research efforts in nanomaterial-mediated colorimetric assays are still required in order to take advantage of their potential for quantitative POC analysis. Along with color changes in these colorimetric assays, nanomaterial-mediated photophysical changes usually occur simultaneously, such as the redshift of the optical absorption peak of the colorimetric probes to a longer wavelength or even into the near-infrared (NIR) region of the electromagnetic spectrum.[23,31,34] For instance, the optical absorption phenomenon occurs in the NIR region in the HRP- or iron oxide NPs-catalyzed TMB-H_2O_2 colorimetric system,[36] but the photothermal effect of this TMB-H_2O_2 colorimetric system has never been explored. With the rapid development of photophysical and nanomaterial science, these significant optical properties might provide new opportunities to explore novel photothermal probes and photothermal immunoassay strategies.

The exploration of new physical and chemical properties of materials is crucial to advance analytical chemistry and material science and to expand their new applications.[3] Herein, we, for the first time, explored the photothermal effect of the iron oxide NPs-mediated TMB-H_2O_2 colorimetric system, and applied it to develop a new simpler NP-mediated photothermal immunoassay platform using a common thermometer as the quantitative signal reader, without complicated material conversion procedures. Using a sandwich-type proof-of-concept immunoassay, the iron oxide NPs-labeled antibody was used as the detection antibody. Due to their peroxidase-mimicking activity, iron oxide NPs captured in the immunoassay system were employed as the artificial HRP to catalyze the TMB-H_2O_2 colorimetric reaction, as shown in Scheme 1. The iron oxide

Scheme 1. Schematic Illustration of the Photothermal Immunoassay Platform Based on the Photothermal Effect of the Iron Oxide NPs-Mediated TMB-H_2O_2 Colorimetric System

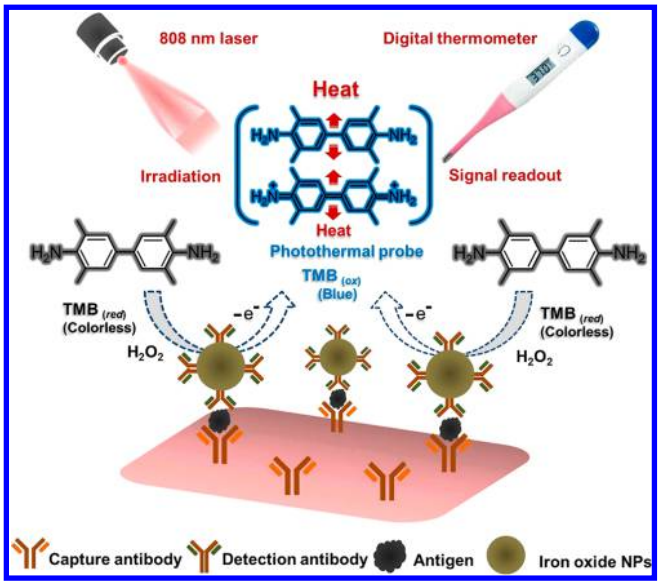

NPs-mediated colorimetric product, the charge transfer complex of the one-electron oxidation product of TMB (oxidized TMB), exhibited not only color changes in the immunoassay, but also a strong NIR laser-driven photothermal effect. Thus, oxidized TMB as a traditional colorimetric probe also acted as a highly sensitive photothermal probe to convert the immunoassay signal into heat through its photothermal effect, thereby allowing sensitive and quantitative photothermal immunoassay using just a thermometer for the visual signal readout. Using the new iron oxide NPs-mediated TMB-H_2O_2 photothermal immunoassay platform, along with a prostate cancer biomarker, prostate-specific antigen (PSA), as a model analyte, we successfully determined PSA at a lower concentration than the clinical diagnostic threshold (4.0 ng·mL^{-1}).

EXPERIMENTAL SECTION

Materials and Instruments. Prostate-specific antigen (PSA) was purchased from Sigma-Aldrich (Burlington, MA, U.S.A.). Monoclonal mouse antihuman PSA antibody and polyclonal rabbit antihuman PSA antibody were obtained from Abcam (Cambridge, MA, U.S.A.). A diode laser with output power from 0 to 2.5 W was purchased from Opto Engine (Midvale, UT, U.S.A.; model number MDL-III-808; wavelength 808 nm; ∼7 × 17 × 5 cm in dimension; see Supporting Information for details).

Iron Oxide NPs-Mediated TMB-H_2O_2 Photothermal Immunoassay. To monitor the photothermal effect of the Fe_3O_4 NPs-mediated TMB-H_2O_2 colorimetric immunoassay solutions obtained from different PSA concentrations (1.0−64.0 ng·mL^{-1}), the immunoassay solutions (0.15 mL) in PCR tubes (0.2 mL) were irradiated vertically with the laser for 20 s

DOI: 10.1021/acs.analchem.8b00842
Anal. Chem. 2018, 90, 5930−5937

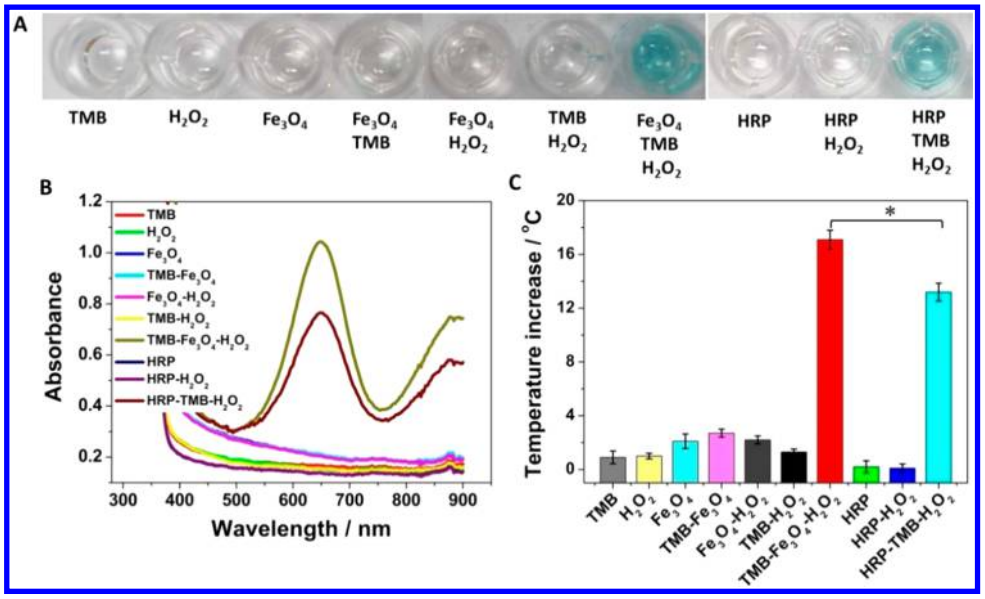

Figure 1. Photographs (A) and UV−vis absorption spectra (B) of different components of the Fe_3O_4 NPs/HRP-mediated TMB-H_2O_2 colorimetric reaction system. (C) Temperature changes (ΔT) of the reaction solutions (0.15 mL) after the irradiation by an 808 nm laser for 20 s at a power density of 5.26 W·cm^{-2}. All temperature increase values are the absolute temperature increment values by comparing the temperature of the solutions before and after the irradiation. The final concentrations of Fe_3O_4 NPs, HRP, TMB, and H_2O_2 in the reaction solutions are 0.006 mg·mL^{-1}, 0.002 U·mL^{-1}, 0.4 mM, and 1.0 M, respectively. Error bars indicate standard deviations (n = 4). An asterisk indicates a statistically significant difference (*P < 0.05).

at a power density of 5.26 W·cm^{-2}. A pen-style digital thermometer probe was immediately inserted into the solutions to monitor the temperature change after the irradiation. The highest steady temperature value achieved after about 5−8 s was recorded as the photothermal measurement signal. It should be noted that the laser power density changed (3.12 or 5.26 W·cm^{-2}) due to different laser irradiation directions and different surface areas under different situations. For example, a glass cuvette was used just to monitor the kinetic process of the photothermal effect over time, while PCR tubes were used for the final quantitative immunoassay (see Supporting Information for more details).

RESULTS AND DISCUSSION

Investigation of Photothermal Effects of the Fe_3O_4 NPs-Mediated TMB-H_2O_2 Colorimetric System. Iron oxide NPs (Fe_3O_4 NPs) have been well established as efficient artificial HRP to catalyze the oxidation of TMB in the presence of H_2O_2.[36] Based on the color change from the oxidation product of TMB, the Fe_3O_4 NPs-mediated TMB-H_2O_2 colorimetric system has been widely used for immunoassays by employing a UV−vis absorption spectrometer as the quantitative signal reader.[36] Along with the color change, it is worth noting that significant changes in optical absorption properties often occur, providing the possibilities for exploration of the photothermal effect of the colorimetric system.

To study the feasibility of the Fe_3O_4 NPs-mediated TMB-H_2O_2 colorimetric system (i.e., with no immunoassays involved) for photothermal conversion, we evaluated the colorimetric, optical, and photothermal properties of the system. Figure 1 shows the photographs, UV−vis absorption spectra, and the 808 nm laser-driven photothermal effect of different components in the colorimetric reaction system. Significantly, a rapid color change from colorless to blue was observed only in the presence of Fe_3O_4 NPs, TMB, and H_2O_2, whereas no apparent color changes were exhibited in other cases without the presence of Fe_3O_4 NPs, TMB, and H_2O_2 (Figure 1A). The resulting blue color indicated the successful Fe_3O_4 NPs-mediated TMB-H_2O_2 colorimetric reaction, where Fe_3O_4 NPs catalyzed the one-electron oxidation of TMB to generate the charge transfer complex of oxidized TMB. To further confirm the above colorimetric reaction, the traditional HRP-catalyzed TMB-H_2O_2 colorimetric reaction was carried out. Similarly, the typical blue color was observed only in the presence of HRP, TMB, and H_2O_2, further confirming the successful Fe_3O_4 NPs (artificial HRP)-mediated TMB-H_2O_2 colorimetric reaction. Strong characteristic absorption peaks were observed at 650 nm in the UV−vis absorption spectra only with the appearance of the blue color in both Fe_3O_4 NPs- and HRP-mediated TMB-H_2O_2 reaction systems (Figure 1B). The absorption peak derives from the charge transfer complex of the one-electron oxidation product of TMB (oxidized TMB) during the colorimetric reactions.[34,36] It is worth noting that the absorbance of oxidized TMB increased drastically from 750 nm in the NIR region, whereas no apparent light absorption was observed when no color changes were present. The significant light absorption of oxidized TMB in the NIR region indicates the possibility of the TMB-H_2O_2 colorimetric system for the NIR laser-driven photothermal conversion.

Similarly, different components from the reaction system were exposed to an 808 nm laser at a power density of 5.26 W·cm^{-2} for 20 s to test the photothermal effect of the colorimetric reaction system. A pen-style digital thermometer was used to measure the temperature of the colorimetric reaction solutions immediately after the irradiation. A dramatic temperature increase was observed only with the appearance of the blue color after the irradiation. After inserting the thermometer probe into the laser-irradiated reaction solutions, the temperature reading increased rapidly and reached its highest steady value after about 5−8 s. To achieve accurate temperature readout for quantitative analysis, the highest steady temperature

DOI: 10.1021/acs.analchem.8b00842
Anal. Chem. 2018, 90, 5930−5937

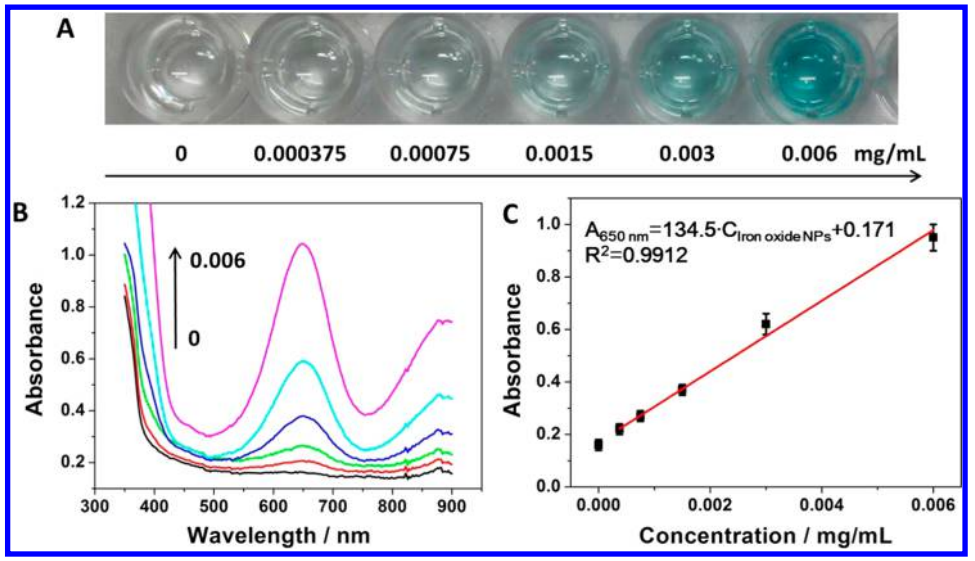

Figure 2. Photographs (A) and UV−vis absorption spectra (B) of the TMB-H_2O_2 colorimetric reaction solutions mediated by different concentrations of Fe_3O_4 NPs in the range from 0 to 0.006 mg·mL^{-1}. (C) Relationship between absorbance (a.u.) at 650 nm in UV−vis absorption spectra of the reaction solutions vs concentration of Fe_3O_4 NPs ($C_{iron\ oxide\ NPs}$ in mg·mL^{-1}). Error bars indicate standard deviations (n = 4).

value was recorded as the photothermal measurement signal. Surprisingly high temperature increases of 17.9 and 13.2 °C were recorded from the Fe_3O_4 NPs- and HRP-mediated TMB-H_2O_2 colorimetric reaction solutions (Figure 1C), respectively, while no significant temperature increases were found in other cases without color changes. These results demonstrated a remarkable NIR laser-driven photothermal effect of the Fe_3O_4 NPs/HRP-mediated TMB-H_2O_2 colorimetric systems, which originated from the charge transfer complex of the one-electron oxidation product of TMB (oxidized TMB) due to its strong light absorption in the NIR region. Similar to some other nanomaterial-based photothermal agents,[37] we believe that the Fe_3O_4 NPs-mediated colorimetric reaction product, oxidized TMB, can act as a photothermal probe to convert the adsorbed NIR light into heat. The discovered photothermal effect may be attributed to the complex photophysical conversion processes of oxidized TMB during the irradiation process. NIR laser-driven photothermal effects of some other small organic molecules have been reported for photothermal therapy of cancers.[38−40] But, to the best of our knowledge, the NIR laser-driven photothermal effect of oxidized TMB has never been reported.

To study the relationship between Fe_3O_4 NPs and oxidized TMB concentrations, the optical absorption properties of the colorimetric reaction system with different concentrations of Fe_3O_4 NPs were then studied, as shown in Figure 2. The colorimetric reaction solutions showed a gradually darkening tendency from colorless to blue as the Fe_3O_4 NPs concentration increased in the range from 0.000375 to 0.006 mg·mL^{-1} (Figure 2A). In addition, the absorbance of oxidized TMB at 650 nm as well as in the NIR region in UV−vis absorption spectra also increased accordingly (Figure 2B). As the Fe_3O_4 NPs concentration increased, their peroxidase-mimicking activity improved, thus leading to the production of a higher concentration of oxidized TMB. It was found that the absorbance at 650 nm was proportional to the concentration of Fe_3O_4 NPs in the range from 0.000375 to 0.006 mg·mL^{-1} with the square of the correlation coefficient of 0.99 (Figure 2C). This linear relationship laid a base to link immunoassay information from Fe_3O_4 NPs to the photothermal effect of oxidized TMB for quantitative biomarker detection.

To study the feasibility of the thermometer-based readout method for quantitative detection of biomolecules, the photothermal effect of the colorimetric reaction solutions mediated by different concentrations of Fe_3O_4 NPs were investigated in detail. The colorimetric reaction solutions were irradiated for different times to monitor the temperature increase, as shown in Figure 3A. As the Fe_3O_4 NPs concentration increased, the temperature of the reaction solutions increased dramatically for the same irradiation times from 10 to 60 s. The result can be attributed to the increasing concentration of the photothermal probe (oxidized TMB) in the reaction solutions. In addition, the temperature elevation rate increased obviously as the irradiation time increased. The temperature increase at shorter irradiation times (10−20 s) was proportional to the concentration of Fe_3O_4 NPs in the range from 0.000375 to 0.006 mg·mL^{-1}, with slopes of 2003.8 °C·(mg·mL^{-1})$^{-1}$ at 10 s and 3058.1 °C·(mg·mL^{-1})$^{-1}$ at 20 s. The result was in good agreement with the linear relationship obtained from the traditional colorimetric study (Figure 2C), indicating the feasibility of the thermometer-based quantitative readout method based on the photothermal effect of oxidized TMB. However, the linear relationship was no longer observed at longer irradiation times (40−60 s), which might be attributed to the photobleaching of oxidized TMB during longer-time irradiation. Thus, 20 s was used as the irradiation time in the subsequent immunoassay study to avoid the photobleaching of the photothermal probe. Fe_3O_4 NPs showed minor temperature increases at both 20 and 60 s, confirming a strong photothermal effect of oxidized TMB.

To further look into the weaker photothermal effect of oxidized TMB during long-time irradiation, a Fe_3O_4 NPs-mediated TMB-H_2O_2 colorimetric reaction solution was irradiated by the laser for 10 min to monitor its photothermal process. A pen-style thermometer probe was inserted into the solution to measure the temperature change during the irradiation. The temperature of the solution increased rapidly from the initial temperature of 24.5 to 38.0 °C within the first 300 s, while no apparent temperature increase was observed in

DOI: 10.1021/acs.analchem.8b00842
Anal. Chem. 2018, 90, 5930−5937

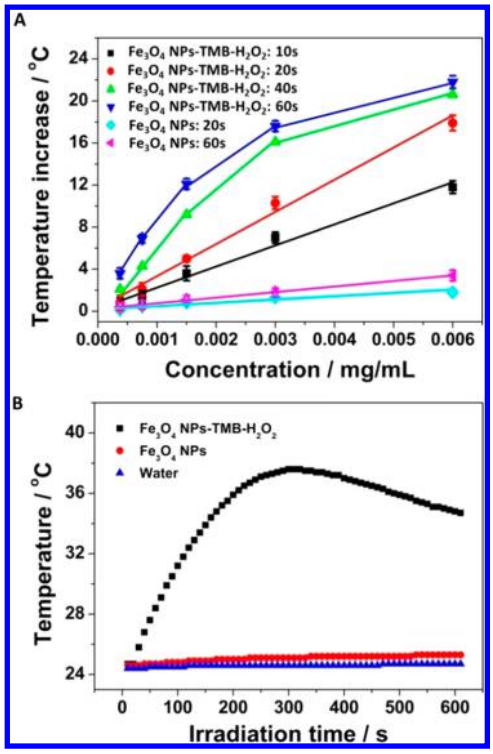

Figure 3. (A) Relationship between Fe_3O_4 NPs concentration (mg·mL^{-1}) and temperature increase (ΔT/°C) of the colorimetric reaction solutions (0.15 mL) after irradiation at a power density of 5.26 W·cm^{-2} for different time periods (10−60 s). (B) Temperature monitoring of the Fe_3O_4 NPs (0.006 mg·mL^{-1})-mediated TMB-H_2O_2 colorimetric reaction solution (1.0 mL), Fe_3O_4 NPs (0.006 mg·mL^{-1}) aqueous dispersion (1.0 mL), and water (1.0 mL) during the 808 nm laser irradiation for 10 min at a power density of 3.12 W·cm^{-2}. Error bars indicate standard deviations (n = 4).

the blank, as shown in Figure 3B. However, the temperature started to decrease after the plateau at around 320 s, indicating a time-dependent decrease in the photothermal effect of oxidized TMB during the longer irradiation process. This phenomenon is different from that of most photothermal nanomaterials, such as Prussian blue-, gold-, and carbon-based nanomaterials,[10−13] which usually show constantly increasing temperature during an irradiation time of 10 min. But a similar time-dependent decrease in the photothermal effect was reported in the case of indocyanine green due to the photobleaching of the organic molecule under NIR laser irradiation.[41−43] Compared with nanomaterials, the photothermal process of small organic molecules is more transient under high intensity irradiation, which could reach a saturated state rapidly within a short irradiation time. As a result, the photothermal effect could not be constantly achieved during long-time irradiation,[41] thereby leading to the decrease of temperature. For comparison, a dispersion of Fe_3O_4 NPs at the same concentration was also irradiated, which exhibited a minor temperature increase of 1.0 °C during the irradiation process. These results further indicated the strong NIR laser-driven photothermal effect of oxidized TMB produced in the colorimetric reaction solution.

Quantification of Disease Biomarkers in Human Serum Using the Fe_3O_4 NPs-Mediated TMB-H_2O_2 Photothermal Immunoassay Platform with a Thermometer. On the basis of the aforementioned studies of the photothermal effect of the Fe_3O_4 NPs-mediated TMB-H_2O_2 colorimetric system, the Fe_3O_4 NPs-mediated photothermal immunoassay platform was then explored using PSA as a model analyte. Normal human serum that was spiked with different concentrations of standard PSA was used for this investigation. After a series of immunoassay reactions and washing steps, as illustrated in Scheme 1, spherical iron oxide NPs were still observed at the substrate surface by the transmission electron microscope (see Supporting Information, Figure S-1), indirectly indicating the successful formation of the sandwich-type immunoassay complex. In addition, the color changes and UV−vis spectroscopic absorbance of these series of final immunoassay solutions were characterized before testing the photothermal immunoassay using a common thermometer. As the PSA concentration increased in the range from 1.0 to 64.0 ng·

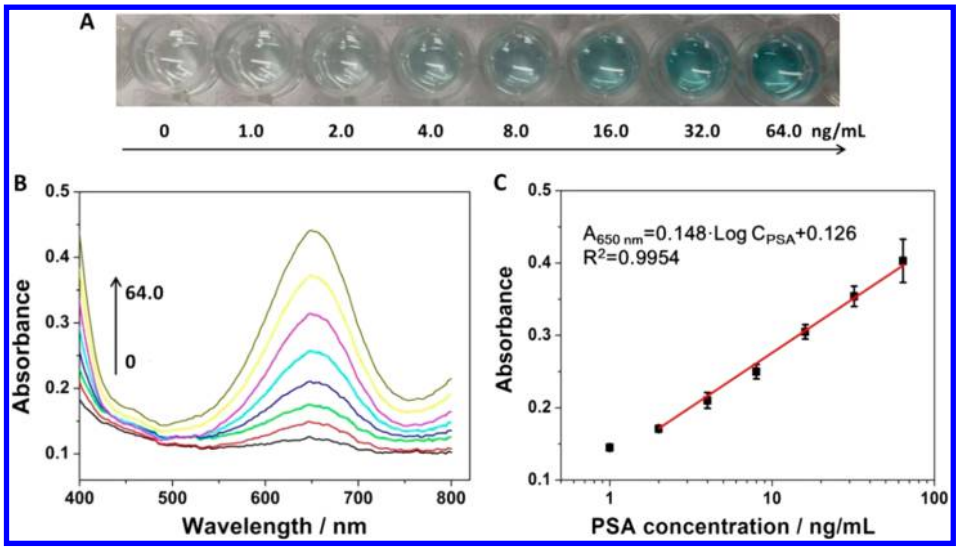

Figure 4. Photographs (A) and UV−vis absorption spectra (B) of the Fe_3O_4 NPs-mediated TMB-H_2O_2 colorimetric immunoassay solutions obtained from different concentrations of PSA in the range from 0 to 64.0 ng·mL^{-1}. (C) Calibration plot of absorbance at 650 nm in UV−vis absorption spectra of the Fe_3O_4 NPs-mediated TMB-H_2O_2 colorimetric immunoassay solutions vs the logarithm of the PSA concentration (C_{PSA}/ng·mL^{-1}). Error bars indicate standard deviations (n = 4).

DOI: 10.1021/acs.analchem.8b00842
Anal. Chem. 2018, 90, 5930−5937

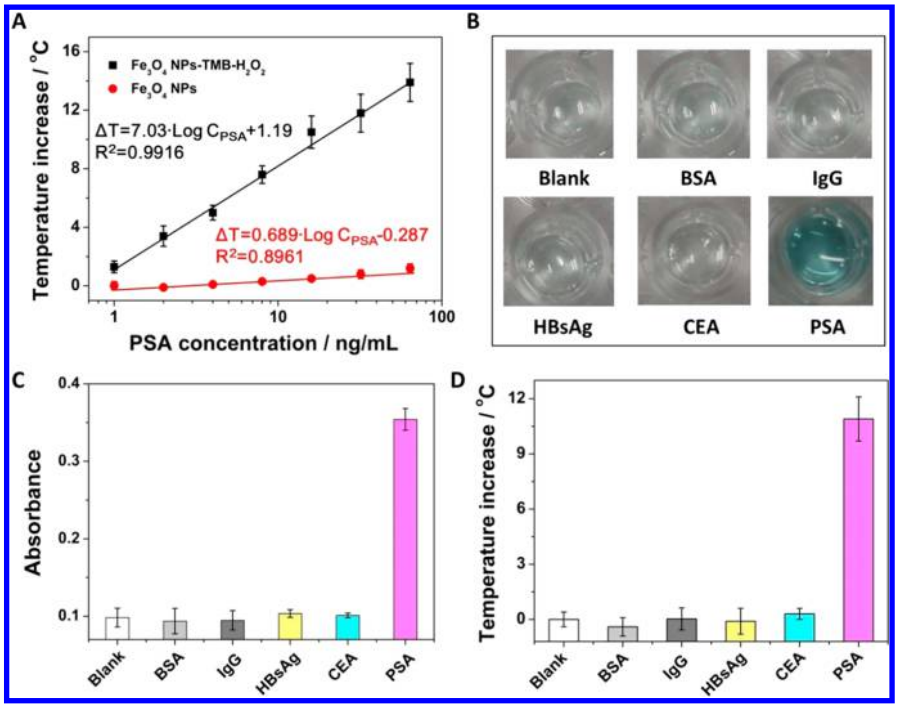

Figure 5. (A) Calibration plots of the temperature increase (ΔT/°C) of the immunoassay solutions in the presence of Fe_3O_4 NPs-TMB-H_2O_2 or in the presence of Fe_3O_4 NPs only vs the logarithm of PSA concentration (C_{PSA}/ng·mL^{-1}). The immunoassay solutions (0.15 mL) were irradiated by the 808 nm laser for 20 s at a power density of 5.26 W·cm^{-2}. (B) Photographs and (C) absorbance at 650 nm in the UV−vis absorption spectra of the Fe_3O_4 NPs-mediated TMB-H_2O_2 colorimetric immunoassay solutions obtained from PSA (32.0 ng·mL^{-1}) and different interfering substances (320 ng·mL^{-1}). (D) Temperature increases of the immunoassay solutions after the laser irradiation. Error bars indicate standard deviations (n = 4). Abbreviations: BSA, bovine serum albumin; CEA, carcino-embryonic antigen; HBsAg, hepatitis B surface antigen; IgG, immunoglobulin G.

mL^{-1}, the immunoassay solutions exhibited a gradually darkening tendency from colorless to blue, as shown in Figure 4A. The result indicated the concentration increase of the photothermal probe (oxidized TMB) in the immunoassay solutions as the PSA concentration increased. In addition, the absorbance of oxidized TMB at 650 nm as well as in the NIR region in the UV−vis absorption spectra of the immunoassay solutions increased as the PSA concentration increased (Figure 4B). The absorbance at 650 nm was proportional to the logarithm of the PSA concentration in the range from 2.0 to 64.0 ng·mL^{-1}, with the square of the correlation coefficient of 0.99 (Figure 4C). Although the color changes from Figure 4A can be used for qualitative or semiquantitative analysis, a UV−vis absorption spectrometer is usually required to accurately quantify the PSA concentrations in serum samples.

We then quantitatively detected PSA using the Fe_3O_4 NPs-mediated TMB-H_2O_2 photothermal immunoassay platform with a thermometer. The immunoassay solutions were irradiated with the laser for 20 s, and their temperature values were recorded to correlate with the PSA concentrations. The temperature elevation increased dramatically with the increase of PSA concentration after the irradiation, as shown in Figure 5A. With the increase of the PSA concentration, more Fe_3O_4 NPs were captured in the sandwich-type immunoassay system, thus resulting in the generation of higher concentrations of the Fe_3O_4 NPs-mediated oxidation product of TMB (photothermal probe) in the immunoassay solutions. Significantly, a high temperature increase of 13.5 °C was monitored at the PSA concentration of 64.0 ng·mL^{-1}, while an obvious temperature increase of 1.4 °C was observed even at 1.0 ng·mL^{-1}. Only slight temperature increases were observed in the absence of TMB and H_2O_2 in the immunoassay system. These results demonstrated the successful transduction of the immunoassay signal into the temperature reading by the Fe_3O_4 NPs-mediated photothermal immunoassay platform, thereby allowing the sensitive visual readout of PSA concentrations using a thermometer. Henceforth, a new simple Fe_3O_4 NPs-mediated TMB-H_2O_2 photothermal immunoassay platform using only a common thermometer will become feasible as a visual quantitative signal reader.

In the PSA concentration range from 1.0 to 64.0 ng·mL^{-1}, as shown in Figure 5A, the temperature increase was linearly correlated with the logarithm of PSA concentrations with the square of the correlation coefficient of 0.99 (ΔT(°C) = 7.03·Log C_{PSA}(ng·mL^{-1}) + 1.19). This linear relationship between the temperature increase and the logarithm of PSA concentration correlates well with the linear relationship between the absorbance and the logarithm of PSA concentration obtained from the traditional colorimetric immunoassay (Figure 4C). Using the new Fe_3O_4 NPs-mediated TMB-H_2O_2 photothermal immunoassay platform with a common thermometer for visual quantitative readout, the limit of detection (LOD) of 1.0 ng·mL^{-1} PSA was determined using three folds standard deviation above the blank (i.e., normal human serum). It should be noted that this LOD is higher than that of some fluorescent and electrochemical methods (1.0−140.0 pg·mL^{-1}),[44−46] but it is comparable to the previously reported traditional ELISA method (1.0 ng·mL^{-1}) using expensive and bulky spectrometers as the quantitative signal reader.[34] It has been reported that the diagnostic threshold concentration of total PSA in human serum is 4.0 ng·mL^{-1} in clinical prostate cancer diagnosis.[34,47] Therefore, this new photothermal immunoassay platform meets the demand of prostate cancer diagnosis in practical clinical diagnostics. Herein, 808 nm was

DOI: 10.1021/acs.analchem.8b00842
Anal. Chem. 2018, 90, 5930−5937

used as the irradiation wavelength because it has been widely used as the representative model wavelength for the investigation of the NIR laser-driven photothermal effect.[11,12] However, the photothermal detection sensitivity might be further improved at other irradiation wavelengths, such as at the absorption peak at 650 nm and even at 980 nm in the longer NIR region, due to the stronger absorbance of the photothermal probe at these wavelengths, which is being further investigated by our group.

Specificity and Reproducibility of the Fe_3O_4 NPs-Mediated TMB-H_2O_2 Photothermal Immunoassay Platform. To study the specificity of the Fe_3O_4 NPs-mediated TMB-H_2O_2 photothermal immunoassay for determining the target PSA, different interfering biomolecules such as BSA, IgG, CEA, and HBsAg were also measured using both the colorimetric and photothermal immunoassay, as shown in Figure 5B–D. No apparent temperature change was observed for the interfering biomolecules even at 10-fold higher concentrations than PSA, while a dramatic temperature elevation of 10.9 °C was recorded for the target PSA (32.0 ng·mL^{-1}; Figure 5D). Additionally, significant color change and a characteristic absorption peak of oxidized TMB at 650 nm in UV–vis absorption spectra were observed only for the target PSA (Figure 5B,C). These results demonstrated high specificity of the Fe_3O_4 NPs-mediated TMB-H_2O_2 photothermal immunoassay in the presence of high concentrations of interfering substances.

To study the reproducibility of the Fe_3O_4 NPs-mediated TMB-H_2O_2 photothermal immunoassay, the temperature increase of six immunoassay solutions at the same PSA concentration was tested. The relative standard deviation (RSD) of the temperature increase from these six immunoassay solutions was 5.12%. Furthermore, five immunoassay solutions at the same PSA concentration were individually obtained and tested at different times over a period of 5 weeks (once a week). The RSD of temperature increase was 6.20% over the time period of 5 weeks. These results demonstrated good reproducibility of the Fe_3O_4 NPs-mediated TMB-H_2O_2 photothermal immunoassay. It should be noted that the photothermal measurement might be slightly affected by the starting temperature of the immunoassay solutions and the surrounding ambient temperature. Nevertheless, the ambient temperature variation can be ruled out, because we used the photothermal effect-induced temperature difference (or the absolute increment value) between immunoassay solutions and the negative control as the final readout signal.

CONCLUSIONS

In this article, we presented our discovery of the photothermal effect of the Fe_3O_4 NPs-mediated TMB-H_2O_2 colorimetric system, and applied it to develop a new simple photothermal immunoassay platform using a common thermometer as the visual signal reader for sensitive and quantitative biomolecular detection. In comparison with our previous work,[29] the new iron oxide NPs-mediated TMB-H_2O_2 photothermal immunoassay platform provides new opportunities for simpler biomolecular quantitation (e.g., no needs for complex NP transformation procedures). The thermometer-based readout method exhibits extraordinary advantages for instrument-free bioanalysis in low-resource settings.[48] Using this method, a cancer biomarker (e.g., PSA) can be readily quantified using a thermometer for rapid cancer diagnosis and screening at various venues such as a physician's office. However, there are still some limitations. For instance, the light source that we used herein is still relatively expensive compared to a thermometer. Nevertheless, with the rapid advancements of photoelectric devices, more and more hand-held NIR laser pointers with different wavelengths and powers are becoming commercially available and affordable (e.g., at a price of ~$100 and lower) to even a physician's office. Given the fact that the TMB-H_2O_2-based colorimetric system is one of the most widely used traditional immunoassays using a UV–vis absorption spectrometer as the signal reader, the newly discovered photothermal effect of the colorimetric immunoassay system shows great potential for POC biomolecular detection and other biomedical and material applications.

ASSOCIATED CONTENT

Supporting Information

The Supporting Information is available free of charge on the ACS Publications website at DOI: 10.1021/acs.analchem.8b00842.

Additional experimental details, results, and discussion (PDF).

AUTHOR INFORMATION

Corresponding Author

*E-mail: xli4@utep.edu.

ORCID

XiuJun Li: 0000-0002-7954-0717

Notes

The authors declare no competing financial interest.

ACKNOWLEDGMENTS

We are grateful for the financial support from the National Institute of Allergy and Infectious Disease of the NIH (R21AI107415), the National Institute of General Medical Sciences of the NIH (SC2GM105584), and the U.S. NSF-PREM Program (DMR 1205302). Financial support from the Emily Koenig Meningitis Fund and Philadelphia Foundation, the NIH RCMI Pilot Grant, the Medical Center of the Americas Foundation, the NIH BUILDing Scholar Summer Sabbatical Award (NIGMS Award numbers RL5GM118969, TL4GM118971, and UL1GM11897), the University of Texas at El Paso for the IDR Program, and the University of Texas system for the STARS Award is also gratefully acknowledged. We are also grateful to Mr. Jeffrey Gonzalez and Dave Primm for help in the manuscript preparation.

REFERENCES

(1) Chen, X.; Chen, Y. T.; Yan, M.; Qiu, M. *ACS Nano* **2012**, *6*, 2550–2557.

(2) Yang, J. P.; Shen, D. K.; Zhou, L.; Li, W.; Li, X. M.; Yao, C.; Wang, R.; El-Toni, A. M.; Zhang, F.; Zhao, D. Y. *Chem. Mater.* **2013**, *25*, 3030–3037.

(3) Katla, S. K.; Zhang, J.; Castro, E.; Bernal, R. A.; Li, X. *ACS Appl. Mater. Interfaces* **2018**, *10*, 75–82.

(4) Huang, P.; Lin, J.; Li, W. W.; Rong, P. F.; Wang, Z.; Wang, S. J.; Wang, X. P.; Sun, X. L.; Aronova, M.; Niu, G.; Leapman, R. D.; Nie, Z. H.; Chen, X. Y. *Angew. Chem., Int. Ed.* **2013**, *52*, 13958–13964.

(5) Yang, K.; Xu, H.; Cheng, L.; Sun, C. Y.; Wang, J.; Liu, Z. *Adv. Mater.* **2012**, *24*, 5586–5592.

(6) Fazal, S.; Jayasree, A.; Sasidharan, S.; Koyakutty, M.; Nair, S. V.; Menon, D. *ACS Appl. Mater. Interfaces* **2014**, *6*, 8080–8089.

(7) Lv, R. C.; Yang, P. P.; He, F.; Gai, S. L.; Yang, G. X.; Lin, J. *Chem. Mater.* **2015**, *27*, 483–496.

DOI: 10.1021/acs.analchem.8b00842
Anal. Chem. 2018, 90, 5930–5937

(8) Lin, M.; Wang, D.; Liu, S.; Huang, T.; Sun, B.; Cui, Y.; Zhang, D.; Sun, H.; Zhang, H.; Sun, H.; Yang, B. *ACS Appl. Mater. Interfaces* **2015**, *7*, 20801−20812.
(9) Li, J.; Wang, W. J.; Zhao, L.; Rong, L.; Lan, S. J.; Sun, H. C.; Zhang, H.; Yang, B. *ACS Appl. Mater. Interfaces* **2015**, *7*, 11613−11623.
(10) Fu, G. L.; Liu, W.; Li, Y. Y.; Jin, Y. S.; Jiang, L. D.; Liang, X. L.; Feng, S. S.; Dai, Z. F. *Bioconjugate Chem.* **2014**, *25*, 1655−1663.
(11) Fu, G. L.; Liu, W.; Feng, S. S.; Yue, X. L. *Chem. Commun.* **2012**, *48*, 11567−11569.
(12) Ke, H. T.; Wang, J. R.; Dai, Z. F.; Jin, Y. S.; Qu, E. Z.; Xing, Z. W.; Guo, C. X.; Yue, X. L.; Liu, J. B. *Angew. Chem., Int. Ed.* **2011**, *50*, 3017−3021.
(13) Moon, H. K.; Lee, S. H.; Choi, H. C. *ACS Nano* **2009**, *3*, 3707−3713.
(14) Zheng, X. H.; Xing, D.; Zhou, F. F.; Wu, B. Y.; Chen, W. R. *Mol. Pharmaceutics* **2011**, *8*, 447−456.
(15) Lv, R. C.; Zhong, C. N.; Li, R. M.; Yang, P. P.; He, F.; Gai, S. L.; Hou, Z. Y.; Yang, G. X.; Lin, J. *Chem. Mater.* **2015**, *27*, 1751−1763.
(16) Fredriksson, S.; Dixon, W.; Ji, H.; Koong, A. C.; Mindrinos, M.; Davis, R. W. *Nat. Methods* **2007**, *4*, 327−329.
(17) Dou, M.; Dominguez, D. C.; Li, X.; Sanchez, J.; Scott, G. *Anal. Chem.* **2014**, *86*, 7978−7986.
(18) Zou, F. M.; Zhou, H. J.; Tan, T. V.; Kim, J.; Koh, K.; Lee, J. *ACS Appl. Mater. Interfaces* **2015**, *7*, 12168−12175.
(19) Guerreiro, J. R.; Frederiksen, M.; Bochenkov, V. E.; De Freitas, V.; Sales, M. G.; Sutherland, D. S. *ACS Nano* **2014**, *8*, 7958−67.
(20) Vashist, S. K.; Schneider, E. M.; Luong, J. H. T. *Analyst* **2014**, *139*, 2237−2242.
(21) Qin, X. L.; Xu, A. G.; Liu, L.; Deng, W. F.; Chen, C.; Tan, Y. M.; Fu, Y. C.; Xie, Q. J.; Yao, S. Z. *Chem. Commun.* **2015**, *51*, 8540−8543.
(22) Akhavan-Tafti, H.; Binger, D. G.; Blackwood, J. J.; Chen, Y.; Creager, R. S.; de Silva, R.; Eickholt, R. A.; Gaibor, J. E.; Handley, R. S.; Kapsner, K. P.; Lopac, S. K.; Mazelis, M. E.; McLernon, T. L.; Mendoza, J. D.; Odegaard, B. H.; Reddy, S. G.; Salvati, M.; Schoenfelner, B. A.; Shapir, N.; Shelly, K. R.; Todtleben, J. C.; Wang, G. P.; Xie, W. H. *J. Am. Chem. Soc.* **2013**, *135*, 4191−4194.
(23) Qu, W. S.; Liu, Y. Y.; Liu, D. B.; Wang, Z.; Jiang, X. Y. *Angew. Chem., Int. Ed.* **2011**, *50*, 3442−3445.
(24) Dou, M.; Sanjay, S. T.; Benhabib, M.; Xu, F.; Li, X. *Talanta* **2015**, *145*, 43−54.
(25) Sanjay, S. T.; Fu, G. L.; Dou, M. W.; Xu, F.; Liu, R. T.; Qi, H.; Li, X. J. *Analyst* **2015**, *140*, 7062−7081.
(26) Petryayeva, E.; Algar, W. R. *RSC Adv.* **2015**, *5*, 22256−22282.
(27) Sun, J. S.; Xianyu, Y. L.; Jiang, X. Y. *Chem. Soc. Rev.* **2014**, *43*, 6239−6253.
(28) Sanjay, S. T.; Dou, M.; Sun, J.; Li, X. *Sci. Rep.* **2016**, *6*, 30474.
(29) Fu, G.; Sanjay, S. T.; Dou, M.; Li, X. *Nanoscale* **2016**, *8*, 5422−7.
(30) Fu, G.; Sanjay, S. T.; Li, X. *Analyst* **2016**, *141*, 3883−3889.
(31) Xia, F.; Zuo, X. L.; Yang, R. Q.; Xiao, Y.; Kang, D.; Vallee-Belisle, A.; Gong, X.; Yuen, J. D.; Hsu, B. B. Y.; Heeger, A. J.; Plaxco, K. W. *Proc. Natl. Acad. Sci. U. S. A.* **2010**, *107*, 10837−10841.
(32) Liu, P.; Yang, X. H.; Sun, S.; Wang, Q.; Wang, K. M.; Huang, J.; Liu, J. B.; He, L. L. *Anal. Chem.* **2013**, *85*, 7689−7695.
(33) Zhou, G. H.; Liu, Y. Z.; Luo, M.; Xu, Q. F.; Ji, X. H.; He, Z. K. *ACS Appl. Mater. Interfaces* **2012**, *4*, 5010−5015.
(34) Gao, Z. Q.; Hou, L.; Xu, M. D.; Tang, D. P. *Sci. Rep.* **2015**, *4*, 3966.
(35) Andresen, H.; Mager, M.; Griessner, M.; Charchar, P.; Todorova, N.; Bell, N.; Theocharidis, G.; Bertazzo, S.; Yarovsky, I.; Stevens, M. M. *Chem. Mater.* **2014**, *26*, 4696−4704.
(36) Woo, M. A.; Kim, M. I.; Jung, J. H.; Park, K. S.; Seo, T. S.; Park, H. G. *Int. J. Mol. Sci.* **2013**, *14*, 9999−10014.
(37) Chen, Q.; Wang, C.; Zhan, Z. X.; He, W. W.; Cheng, Z. P.; Li, Y. Y.; Liu, Z. *Biomaterials* **2014**, *35*, 8206−8214.
(38) Shan, G. B.; Weissleder, R.; Hilderbrand, S. A. *Theranostics* **2013**, *3*, 267−274.
(39) Wu, L.; Fang, S. T.; Shi, S.; Deng, J. Z.; Liu, B.; Cai, L. T. *Biomacromolecules* **2013**, *14*, 3027−3033.
(40) Cheng, L.; He, W. W.; Gong, H.; Wang, C.; Chen, Q.; Cheng, Z. P.; Liu, Z. *Adv. Funct. Mater.* **2013**, *23*, 5893−5902.
(41) Spence, G. T.; Hartland, G. V.; Smith, B. D. *Chem. Sci.* **2013**, *4*, 4240−4244.
(42) Zheng, M. B.; Yue, C. X.; Ma, Y. F.; Gong, P.; Zhao, P. F.; Zheng, C. F.; Sheng, Z. H.; Zhang, P. F.; Wang, Z. H.; Cai, L. T. *ACS Nano* **2013**, *7*, 2056−2067.
(43) Bahmani, B.; Bacon, D.; Anvari, B. *Sci. Rep.* **2013**, *3*, 2180.
(44) Chen, X. Q.; Zhou, G. B.; Song, P.; Wang, J. J.; Gao, J. M.; Lu, J. X.; Fan, C. H.; Zuo, X. L. *Anal. Chem.* **2014**, *86*, 7337−7342.
(45) Choi, J. H.; Kim, H. S.; Choi, J. W.; Hong, J. W.; Kim, Y. K.; Oh, B. K. *Biosens. Bioelectron.* **2013**, *49*, 415−419.
(46) Liu, J.; Lu, C. Y.; Zhou, H.; Xu, J. J.; Wang, Z. H.; Chen, H. Y. *Chem. Commun.* **2013**, *49*, 6602−6604.
(47) Lee, J.; Dak, P.; Lee, Y.; Park, H.; Choi, W.; Alam, M. A.; Kim, S. *Sci. Rep.* **2015**, *4*, 7352.
(48) Dou, M. W.; Sanjay, S. T.; Dominguez, D. C.; Liu, P.; Xu, F.; Li, X. *Biosens. Bioelectron.* **2017**, *87*, 865−873.

DOI: 10.1021/acs.analchem.8b00842
Anal. Chem. 2018, 90, 5930−5937